Quartz Crystal Microbalance Measurement of Self-Assembled Micellar Tubules of the Amphiphilic Decyl Ester of D-Tyrosine and Their Enzymatic Polymerization

Kenneth A. Marx,* Tiean Zhou, and Rupmoni Sarma

Center for Intelligent Biomaterials, Department of Chemistry, University of Massachusetts, Lowell, Massachusetts 01854

Amphiphilic decyl derivatives of D-tyrosine self-assemble into long rodlike or tubular aggregate structures in aqueous buffered solution. In this report we demonstrate the novel use of the quartz crystal microbalance (QCM) to measure the presence in solution, and subequent enzymatic polymerization, of long rodlike monomer aggregates of the decyl ester of D-tyrosine (DEDT) as a function of their formation and increasing surface binding level as pH values increase from 3 to 7. From these data, using the Sauerbray equation to calculate the effective elastic mass surface binding of deprotonated DEDT aggregates, a pK_{app} of 8.3 is obtained for the DEDT α-NH_2 group protonation−deprotonation and subsequent aggregation equilibrium. Furthermore, once aggregates are bound to the QCM surface, we initiate and subsequently monitor enzymatic polymerization of the DEDT monomers by horseradish peroxidase through the measurement of significant changes in the quartz crystal frequency and motional resistance. Following the onset of polymerization, the viscoelastic properties of the bound monomer aggregates change. A final polymerized state is achieved in which the altered physical properties of the polymerized rodlike aggregates make the solution immediately above the QCM surface−solution interface behave as a Newtonian fluid, producing a nearly pure viscosity−density energy dissipative effect on the measured crystal frequency and motional resistance values.

Introduction

Aqueous enzymatic polymerizations are receiving increasing attention as attractive alternatives to traditional methods of polymer synthesis involving free radical initiators in organic solvents. One enzyme that has received considerable attention because of its availability, stability, and wide substrate range is horseradish peroxidase (HRP) (*1*). Phenol derivatives represent an industrially important class of substrates for HRP. Catalysis of reactions of phenols has been carried out with HRP in a number of formats including aqueous solution, organic solvents, reverse micelles, and at the air−water interface in Langmuir−Blodgett (LB) troughs (*2*−*11*).

A serious practical problem associated with phenolic polymers is the difficulty in processing them following synthesis. This is due to insolubility resulting from interchain cross-linking. By contrast, alkyl derivatives of phenols are more easily processed. Recently, we have demonstrated that amphiphilic decyl ester derivatives of D-tyrosine can be polymerized using HRP in aqueous solution, rather than in reverse micelles (*10*). This is accomplished by forming rodlike aggregate structures in aqueous solution, where the phenolic moieties are presumably oriented outward toward the solution and the HRP and are thereby accessible to the enzyme either in the aggregate or, alternately, via an equilibrium exchange where the monomer becomes available in solution.

We have also demonstrated the existence of these long self-assembled DEDT aggregate structures using SEM and measured with light scattering the critical micelle concentration (cmc) and spectrophotometrically the kinetics of polymerization of the monomers, self-assembled in the aggregates (*12*). Very similar rodlike self-assembled aggregates have been observed in a number of small molecule amphiphilic systems (*13*).

The quartz crystal microbalance (QCM) is a surface technique based upon the piezoelectric effect, in which mass and viscoelastic behavior can be distinguished at the solution interface and within a few micrometers above an AT cut quartz crystal. By applying an alternating field across the quartz crystal through an upper and lower metal electrode covering the quartz surface, an oscillation frequency is produced in the crystal. An increase in elastic mass bound to the quartz surface causes the oscillation frequency to shift. For this situation, the Sauerbray equation has been used to precisely quantify, with a detection sensitivity in nanograms, the mass added to the surface (*14*).

Although early applications of QCM were to measuring mass binding to the quartz surface from species in the gas phase, more recently, solution-based QCM has been developed as a tool in analytical chemistry and electrochemistry because of its ability to sensitively measure mass changes associated with liquid−solid interfacial phenomena (*15*−*18*), particularly at electrodes. A number

* Corresponding author. Telephone: (978) 934-3658. Fax: (978) 934-3013. E-mail: Kenneth_Marx@uml.edu.

10.1021/bp990038j CCC: $18.00
Published on Web 04/17/1999

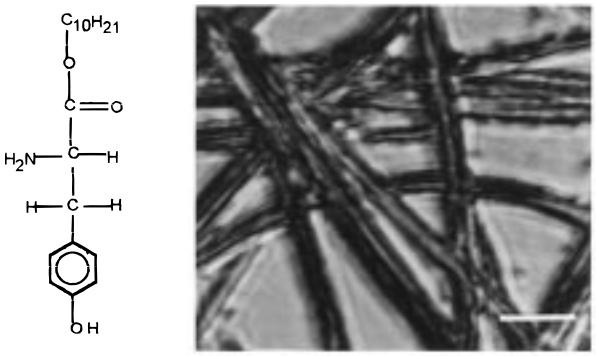

Figure 1. DEDT monomer: (a) chemical structure of decyl ester D-tyrosine; (b) light microscope image of DEDT monomer aggregates at pH 6.0 (bar equals 25 μm).

of excellent reviews of this technique have appeared (*19*−*21*). Viscosity−density changes in the solution above a QCM crystal surface can produce significant frequency (*f*) and motional resistance (*R*) shifts. These viscosity−density alterations can also be brought about by viscoelastic behavior of systems bound to or in the solution layer immediately above the QCM surface. Methods to distinguish viscosity−density solution effects on the crystal from surface bound elastic mass shifts have been described (*22*−*24*).

QCM has been applied sporadically as a biosensor, where biological macromolecules have been incorporated into the sensing system design. In a few instances, measurements were made of fundamental biological processes such as blood clotting kinetics (*25*, *26*), DNA reassociation (*27*, *28*), DNA chemical modification by cisplatin (*29*), Hoechst 33258 drug intercalation into DNA (*30*), and immunological reactions (*31*−*33*). In other systems, the QCM has been used to detect lipopolysaccharide binding peptides or antibiotics binding to lipopolysaccharides bound to the QCM surface (*34*,*35*), as an affinity sensor where self-assembling thiols can be used to coat and modify the gold QCM surface (*36*), and as a total urinary protein sensor (*37*).

Whole cells can be monitored when they are bound to the QCM surface (*38*−*41*). In another study, we have used the QCM to describe the time-dependent sequence of initial contact, subsequent adhesion, and spreading of normal bovine endothelial cells as they sediment to the QCM surface, then contact and flatten out while forming putative extracellular matrix binding contacts on the QCM surface (*42*).

The mass and viscoelastic sensing features of the QCM technique make it attractive to apply to our system comprised of large anisotropic self-assembling rodlike aggregates. In this report, we demonstrate a novel application for the QCM technique in which the frequency and motional resistance measurements provide information that supports the existence and QCM surface binding level of the self-assembled aggregates. Furthermore, QCM measures the altered viscosity−density properties of the solution surface above the crystal, brought about by the altered viscoelastic properties of the aggregates following their enzymatic polymerization with HRP.

Materials and Methods

Polymerization Reaction and Light Microscopy. The DEDT was prepared as described elsewhere (*10*). The structure of this monomer is shown in Figure 1a.

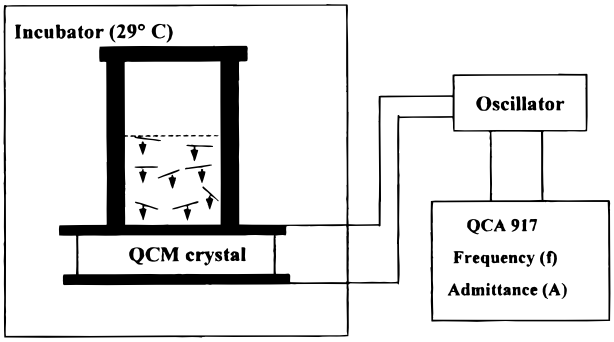

Figure 2. Schematic diagram of the QCM cell inside a constant temperature incubator and associated Δf and ΔR measurement apparatus. The diagram indicates the sedimentation of rodlike aggregates to the QCM surface.

Horseradish peroxidase RZ 3.0 was purchased from Sigma Chemical Co. and hydrogen peroxide (30% solution) from Aldrich Chemical Co. A DEDT solution was prepared immediately before each experiment as follows. The DEDT monomer, 0.31 mM in water, was solubilized by being brought to pH 3 through the addition of dilute HCl. For each experiment at varying pH values, the solution was brought to the final pH through the addition of small volumes of 1 M dibasic sodium phosphate. For light microscopy, a pH 6.0 solution was allowed to stand for 1 h; the solution was then dried on a glass slide and photographed with an Olympus C-35AD camera under illumination in an Olympus BH-2 microscope.

Quartz Crystal Microbalance. An AT cut quartz crystal of resonant frequency 8.846 MHz with a gold electrode (5 mm diameter) was used in a cylindrical Teflon cell. The crystal was sandwiched between two O-rings to allow only one side of the electrode to be exposed to the solution (Figure 2). The device was placed inside a temperature-regulated incubator. A Model QCA 917 quartz crystal analyzer system (Seiko EG&G), comprised of a main unit and oscillator, was used for the simultaneous measurement of the resonant frequency (*f*) and resonance admittance (*A*). First, the stable *f* and *A* values in pure water were recorded. Then the water was removed from the cell, and the cell was rinsed with the DEDT-containing stock solution followed by addition of the pH-adjusted 300 μL of DEDT stock solution (described above) to the cell. Then the upper end of the cell was covered with a polystyrene plate. This prevented evaporation of water from the cell along with the fact that the incubator was humidified with a reservoir of distilled water. Oscillation is known to occur about the invariant equilibrium frequency value if the pressure is changing due to evaporation changing the solution column length above the QCM crystal surface. The fact that no significant frequency oscillation was detected in our studies indicates that there was no change in solution volume or column length above the QCM during the course of these experiments.

Values of *f* and *A* were monitored over one to several days following the sedimentation and binding of the aggregates to the gold QCM surface. No pH drift was observed over the course of these experiments, since pH values were checked with a pH meter before and after completion of the QCM experiments. In experiments where polymerization was carried out, 10 units of HRP enzyme was added in a small volume of sodium phosphate buffer with a pH identical to that of the DEDT solution. Hydrogen peroxide was added in varying volumes as a 0.08 mM solution in water. The admittance,

A (in μS), was converted into motional resistance, R (in Ω), using the relationship $R = 10^6/A$.

Results and Discussion

Measuring pH-Dependent DEDT Aggregation. In previous studies, we have presented preliminary investigations of the ability of the DEDT monomer to both form aggregates (*11*) and to undergo polymerization by HRP (10). Early studies of the polymerization reactions of DEDT led us to visualize these aggregates because we observed anecdotally that, upon forming a near-neutral pH stock solution of the monomer, visible yellow brownish needlelike aggregates would appear and settle out in the container with time, at a rate that was both concentration- and pH-dependent. Recently, we measured the cmc values for DEDT monomers to be 0.23 mM at pH 5.5 and 0.17 mM at pH 6.0 (*12*). That these monomers form macroscopic tubule structures above the cmc can be seen in Figure 1b. Here, we present a light microscope image of tubules of self-assembled DEDT monomer above the cmc. The tubules vary in size around 5 μm diameter and >200 μm length. Identical structures were observed with the L-isomer (DELT). Therefore, we confined our QCM study to the DEDT isomer.

Given that we have evidence for both aggregate structures and their polymerization using HRP, we decided to study these properties of this system using the QCM technique. QCM is particularly well-suited to this because micellar tubule structures binding to the gold QCM surface should produce a measurable frequency shift in the underlying quartz crystal. Furthermore, the long rodlike aggregates could be expected to alter the solution viscosity−density and therefore the crystal motional resistance, R, at the gold electrode−solution interface.

The Figure 2 schematic diagram depicts the sedimentation process of DEDT monomer aggregates to the QCM surface, a process we investigated as a function of pHs from 3 to 7. While the exact pK_a of the amine group in DEDT is unknown, the tyrosine α-NH_2 group's pK_a is 9.1 (*43*). Since DEDT contains an esterified −COOH, in contrast to the −COOH group in tyrosine, the DEDT α-NH_2 pK_a should be shifted to a lower value. Over the increasing pH 3−7 range, the monomers undergo a protonation−deprotonation equilibrium. This results in a transition from a + charged monomer to an uncharged monomer with increasing pH, which should allow the amphiphilic monomers to undergo self-assembly into micelles. This property has been observed for other amphiphilic molecules going from the charged to the uncharged state (*13*). We have demonstrated that, upon going from the lower to higher pH value, the DEDT aggregates increase in size, starting initially as small spherical micelles, then transitioning to rod- or tube-shaped structures (*12*). That the cmc value decreases with increasing pH, as mentioned above, reflects this phenomenon.

Using different pH values between 3 and 7, in Figure 3, we measured the kinetics of the quartz crystal frequency decrease resulting from the DEDT monomer aggregates sedimenting to and binding the gold surface of the QCM (schematic in Figure 2) in the four separate experiments shown. There is a sharp initial f decline in the first few minutes, especially for the highest studied pH of 6.99, where Δf goes from 0 Hz for pure buffer to 280 Hz at $t = 0$ and to 480 Hz at $t = 18$ s, following DEDT addition to the QCM cell. The earliest part of this fast time regime is not clearly resolved, being within the dead time of our measurement system. Following this, there is a steadily increasing rate of decline in f with increasing pH. The exception is at a low pH of 3.0, where little change is observed in f. This is what we would expect from the absence of aggregates observed at pH 3.0 and the presence and surface binding of larger aggregates at higher pHs (*12*). Little change in R was observed for the lowest three pH values. For pH 6.99, ΔR began to change significantly (data not shown). This R change suggests that the aggregates begin to exhibit viscoelastic behavior, producing altered solution properties exhibiting energy dissipative effects upon the crystal, thereby altering the crystal motional resistance. We examine the change in R in more detail below in Figure 5.

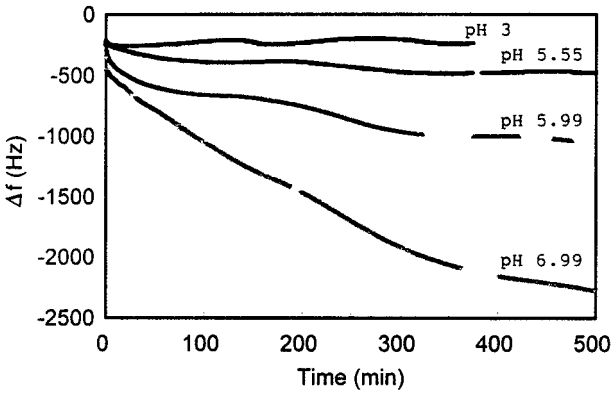

Figure 3. Kinetics of Δf shifts induced by DEDT monomer aggregates binding to the QCM surface at a series of increasing pH values.

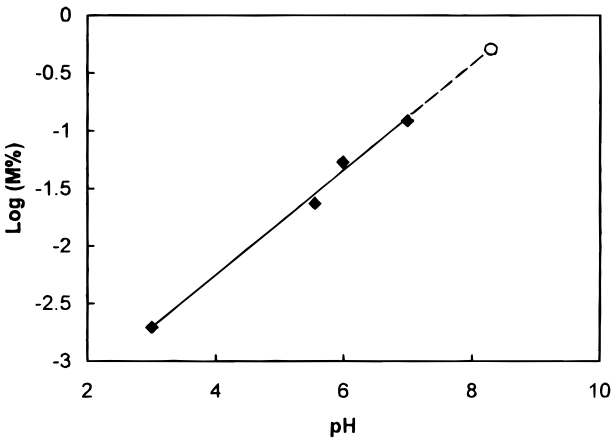

Figure 4. Logarithm of the equilibrium surface-bound DEDT elastic mass (M) aggregate percentages, as a function of pH. Bound masses are calculated using the Sauerbray equation (eq 1). The total DEDT added to the QCM cell represents 100%. Extrapolation (dashed line) is to the point (empty circle) where $(DEDT^{+}_{m}) = (DEDT_{aggr})$.

Frequency shifts may be used to calculate the effective DEDT elastic masses bound to the QCM surface using the Sauerbray equation:

$$\Delta f = -2\Delta m f^2/A(\mu\rho_q)^{0.5} = -C_f\,\Delta m \qquad (1)$$

where Δf is the measured resonant frequency decrease (Hz), f the intrinsic crystal frequency (8 846 000 Hz), Δm the mass change (g), A the electrode area (0.196 cm^2), ρ_q the density of quartz (2.65 g/cm^3), μ the shear modulus (2.95×10^{11} dyn/cm^2), and C_f the integrated sensitivity (0.903 Hz/ng).

On the basis of the above equation and the equilibrium frequency shifts observed at 24 h for DEDT solutions of

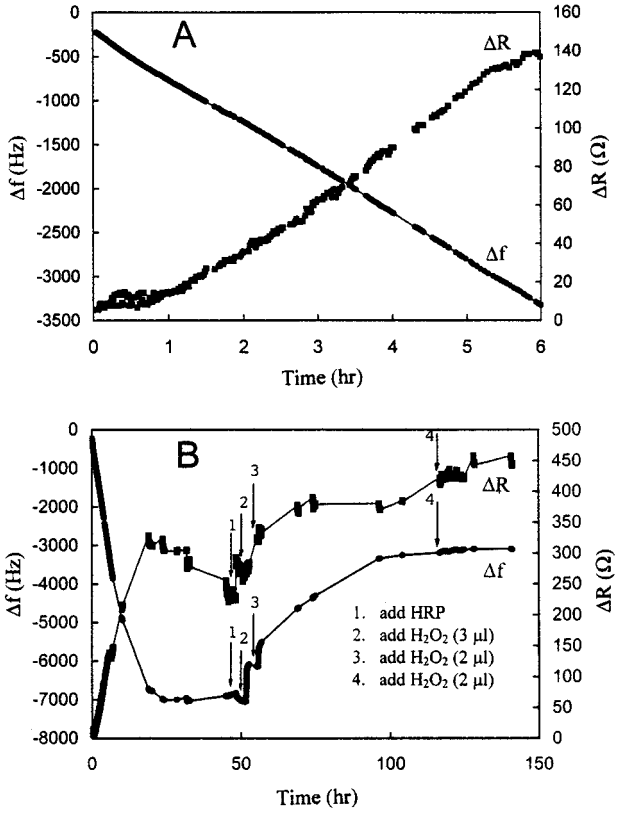

Figure 5. Kinetics of Δf and ΔR shifts induced by DEDT monomer aggregates at pH 7.01: (A) early linear region of sedimentation and binding to the QCM surface; (B) longer time region including equilibrium Δf and ΔR values and how they are affected by HRP polymerization of monomer aggregates at arrows 2−4, where H_2O_2 is added.

different pH, the elastic masses collected on the QCM electrode can be estimated. We present these data in Figure 4. The bound masses, presented as percentages of the total solution mass, range from 0.85% at pH 3.0 to 12.3% at pH 6.99. The latter mass, 3.6 μg, represents a large mass for the QCM crystal to detect. We did not collect data beyond the pH 6.99 mass. This was for two reasons. The first was to avoid a nonlinear response with increasing mass load. Second, incrementally added QCM surface mass, in this rodlike aggregate system, faces a large excluded surface volume problem. Figure 1b shows visually that it takes few randomly positioned rodlike aggregates to completely exclude the QCM surface from further direct binding. Binding must be indirect, mediated at only a few points of contact, through already bound rodlike aggregates.

These Figure 4 data suggest an apparent pK_{app} of about 8.3 for the monomer protonation−deprotonation and aggregation equilibrium, viewed as a simple two state process:

$$DEDT^{+}_{[m]} = DEDT_{[aggr]} + H^{+} \qquad (2)$$

where the DEDT monomer can be in the free solution state [m] or in the tubule aggregate [aggr] state. The pK_{app} value is obtained by estimation, from the point where the data extrapolate to the condition ($DEDT^{+}_{[m]}$) = ($DEDT_{[aggr]}$); see Figure 4. This pK_{app} value does not have a thermodynamically rigorous definition. However, given the uncertainty in applicability of the Sauerbray equation (eq 1) to the Figure 4 data, a rigorous thermodynamic description of this system is not warranted. Our use of the pK_{app} represents a method of interpreting the binding data semiquantitatively, in terms of a simple model. We carry out this interpretation below.

In our system, the pI for DEDT is expected to be the average of the α-NH_2 and −OH pK_a values, or about 9.6 [pI = (8.3 + 10.9)/2]. This should represent the point of lowest solubility of the monomer or highest aggregation level. It is consistent with the increasing bound mass values we measured from pH 3.00 up to pH 6.99. The DEDT pK_{app} we observed at 8.3 is lower than that for tyrosine α-NH_2, which has a pK_a of 9.1. This shift is expected for two reasons. First, the decyl group will tend to drive aggregation, bringing the α-NH_3^+ groups into close proximity, thereby lowering the effective pK_a of this group in DEDT. Second, removing the charged α-COO^- of tyrosine by esterification to form the DEDT derivative, will somewhat destabilize the protonated α-NH_3^+ form of DEDT relative to the amino acid, thereby lowering its pK_a. The direction of this effect is consistent with the observed pK_a downshift of α-NH_2 amino acid groups in an oligoalanine series of different chain lengths as the terminal α-COO^- group is moved further down the chain (*43*).

The phenomenon we observe, increased binding of the neutral DEDT aggregate species, in a form that can be considered insoluble, is very similar to a system previously described (*44*). These investigators created a novel cellular metabolic sensor using an amphiphilic polymer, which increasingly bound to the QCM surface as pH values approached its pI, where the net charge was zero. The QCM Δf shift could then be related to the metabolic rate of the cell population, which generated acidic metabolites that altered the pH.

Enzymatic Polymerization. A major aim of this study was to examine whether the QCM technique was capable of measuring the enzymatic polymerization of these aggregate structures we studied previously (*10*). To examine this possibility we used the high end of the studied pH range, where the aggregates were most abundant and where our Δf and ΔR shift values were of greatest magnitude. We carried out the QCM binding experiment shown in Figure 5 at pH 7.01. Here we observe in panel A that, at the early times in the QCM response, there is a linear decrease in the Δf, and after an initial 1 h of no change, ΔR begins to increase in a nearly linear fashion. We feel that this reflects a physical process in which the aggregate structures sediment to and then bind the QCM surface. Sedimentation to the crystal surface, a linear time-dependent process, would be expected to result in a linear surface mass increase with time, therefore producing the continuous linear Δf change. On the other hand, the lack of ΔR change during the first hour suggests no change in the crystal motional resistance due to solution ρ and η changes. That is, the initial 1 h binding of aggregates results in pure elastic mass binding to the QCM surface.

After the first hour, as ΔR begins to increase, the subsequent sedimentation of aggregates to the surface does not produce pure elastic mass binding but the aggregates begin to alter the solution ρ, η above the crystal. This effect is not unexpected given the physical situation at the QCM surface. As we discussed previously, the initial long rodlike aggregates that bind, due to their random positioning, create a large excluded surface volume for the subsequent binding of aggregates. Aggregates binding at longer times are sterically excluded from direct contact with the surface and must stack randomly on top of the network of previously bound aggregates. The expected result would be an alteration of R, as we observe.

It is clear from Figure 5B that, after the initial 10 h, the Δf decrease and ΔR increase level off to constant equilibrium values by about 24 h. At these times, there is clearly no longer any net sedimentation of aggregates to the QCM surface and we believe the system has achieved equilibrium. At the point labeled 1, we add the HRP enzyme. Addition of HRP and subsequently hydrogen peroxide volumes to the DEDT in the QCM cell were carried out slowly with a micropipet just underneath the solution meniscus to avoid any mixing of the DEDT aggregates at the QCM−liquid interface. At point 2, we added H_2O_2 to the solution to initiate the polymerization reaction. There is clearly a rise in Δf and ΔR. At point 3, another aliquot of H_2O_2 was added followed by a long substantial rise in both Δf and ΔR. At point 4, a final aliquot of H_2O_2 was added, sufficient in previous experiments monitored spectrophotometrically (*10*) to achieve saturation polymerization. This resulted in only small changes to the final values of Δf and ΔR.

The significant increase in f upon polymerization to a final Δf value of around −3000 Hz can be interpreted as a significant loss of aggregate mass bound to the QCM surface upon polymerization. We are not sure of the exact reason for this phenomenon. It may be due to an alteration in surface structure and lowered binding affinity of the aggregates for the QCM surface on going from monomer to polymerized monomers in the final aggregate structure. From SEM observations, we know that the aggregates do not change gross dimensions upon polymerization, although they do become significantly more robust structures mechanically as would be expected following polymerization of the monomers comprising them (*11*, *12*). This fact can help explain the very significant increase in R, which reflects a change in the crystal motional resistance due to increasing energy dissipative solution properties that accompany polymerization of DEDT aggregates above the QCM crystal surface. In the following section we discuss the latter change and how one may interpret these Δf and ΔR changes.

An experiment identical to that in Figure 5 was carried out at a pH of 5.5 (data not shown). At pH 5.5, we observed an identical effect on Δf and ΔR due to polymerization, but of a significantly lesser magnitude. We also performed a control experiment in which HRP was added to the 50 h stable aggregate bound QCM surface. The result was Δf and ΔR values similar to those in Figure 5, prior to polymerization. These quantities did not significantly change over a subsequent 40 h period, even when distilled water was substituted for the H_2O_2 aliquots. Only when H_2O_2 was finally added and polymerization took place did the Δf and ΔR values rise as we observed in Figure 5. This control demonstrates that these significant Δf and ΔR changes are the result of polymerization by the enzyme and not simply the result of a physical interaction of the aggregates with the added enzyme.

The QCM technique reveals clear evidence for the occurrence of the enzymatic reaction in its ability to characterize the altered properties of the oligomeric products in the aggregate structures. However, powerful as it is in this regard, QCM is not suited to following reaction kinetics. To carry out the study of this reaction, mixing was avoided in the solution above the QCM surface, to prevent disturbing the equilibrium surface bound monomer aggregates. Of necessity, this prevented us from any possibility of rapid mixing in order to follow the kinetics of enzymatic polymerization in the aggregates.

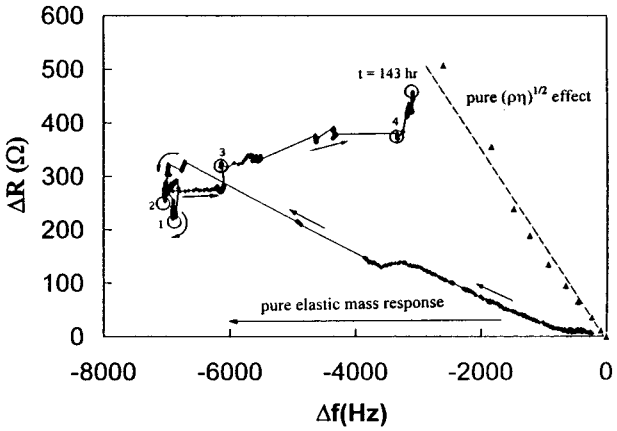

Figure 6. $\Delta f-\Delta R$ diagram of the time course of binding and HRP polymerization of DEDT monomer aggregates at pH 7.01. The time course of the Figure 5 data (filled circles) is indicated by the arrows, starting at the lower right with the $t = 0$ point. When the points reach labeled point 1, HRP was added. At points 2−4, H_2O_2 was added and the final $t = 143$ h point at the end of polymerization is circled. The $\Delta f-\Delta R$ behavior of a pure elastic mass bound at the QCM surface is indicated by the horizontal line. The $\Delta f-\Delta R$ points (filled triangles) determined experimentally for a series of increasing concentration sucrose solutions is depicted with a best linear fit (dashed line). This is the behavior of a Newtonian fluid producing a pure viscosity−density effect on the QCM $\Delta f-\Delta R$ values. QCM behavior intermediate between that of a pure bound elastic mass and a pure viscosity−density solution effect is said to be caused by material exhibiting viscoelastic behavior.

QCM has been employed to measure a related effect of enzymatic reactions in a report on the microrheology of blood clotting (*25*). These investigators recorded the effects on Δf and ΔR of the clotting reaction, which is enzymatically catalyzed. Also, they were able to demonstrate a significant difference in the clotting reaction with and without added urokinase, a fibrinolytic enzyme.

Pure Elastic Mass versus Liquid Viscosity−Density Response. When one face of a quartz crystal is in contact with a liquid, its f and R values are affected by the liquid density and viscosity. Therefore, changes in the f response of a QCM crystal can be brought about independently by both (1) a pure elastic mass response, where mass is bound tightly to the QCM surface, R is constant, and the Sauerbray equation (eq 1) holds and (2) a pure liquid viscosity−density change in the solution adjacent to the QCM surface, bringing about a change in both f and R, the resonant motional resistance.

To determine what type of change is bringing about any given f change, the Δf, ΔR data can be combined in the form of Figure 6. A pure elastic mass binding Δf change has $\Delta R = 0$, as is shown by the horizontal labeled line. A pure liquid viscosity−density response has the f and R behavior shown by the dashed line. This was determined in the following way. The equation for the resulting resonant frequency change was first derived by Kanazawa et al. (*22*) as follows:

$$\Delta f = -f^{3/2}(\rho_L \eta/\pi\mu\rho_q)^{1/2} \qquad (3)$$

where ρ_L is the density of the liquid and η is the viscosity of the liquid. For the quartz crystal in contact with liquid, the resonant resistance change was first derived by Muramatsu et al. (*45*) as follows:

$$\Delta R = (2\pi f \rho_L \eta)^{1/2} A/k^2 \qquad (4)$$

where k is the electromechanical coupling factor. Since

both Δf and ΔR are proportional to $(\rho_L \eta)^{1/2}$, the $\Delta f - \Delta R$ diagram should be a straight line for liquids of different density and viscosity. Therefore, a series of different weight percent (0−46%) sucrose solutions, of varying density and viscosity, were prepared and the f decrease and R increase were determined relative to those of pure water using eqs 3 and 4. These data and fitted dashed line are presented in Figure 6 as the pure density−viscosity response behavior of ΔR, Δf points.

Now we can discuss the Figure 5 kinetic data, displayed in Figure 6, where the time course of ΔR, Δf data points is indicated by the arrows, starting at the bottom right of the figure at time zero. The earliest points have zero slope, and Δf changes with little if any change in ΔR. This is the behavior of a pure elastic mass response obeying the Sauerbray equation (eq 1), where mass is bound to the QCM surface with no change in the crystal motional resistance R, due to invariant solution properties above the QCM crystal. This region is equivalent to the time points less than 1 h in Figure 5A. Following the time arrows, the next points then have a negative slope, characteristic of viscoelastic behavior in the solution above the crystal. The response is little changed going through point 1, where the HRP enzyme was added. However, at point 2, where H_2O_2 is added to the QCM cell to initiate polymerization, a significant change results. Now the Δf, ΔR points change dramatically and move toward the pure $(\rho_L \eta)^{1/2}$ response line. At points 3 and 4, additional H_2O_2 was added so that, at 143 h, where polymerization was complete, the $\Delta f - \Delta R$ values are very close to those of a pure density−viscosity response.

This analysis clearly establishes that enzymatic polymerization brings about a marked change in the rodlike aggregate system that results from polymerization. This system goes from an initial state of bound elastic mass, to subsequently bound aggregates exhibiting viscoelastic behavior, to a final polymerized aggregate behavior that alters the solution properties to produce a largely density−viscosity type of energy dissipative effect on the QCM crystal oscillation. This is the type of behavior that we might expect since density and increasing viscosity changes are likely to accompany the enzymatic conversion of monomers to oligomers in these aggregates.

In unpublished SEM images, we have shown that the unpolymerized tubule aggregates, while similar in morphology and diameter to the polymerized aggregates, are mechanically fragile and are frequently found broken into smaller lengths. This mechanical fragility, producing shorter monomer aggregate lengths, may be responsible for some or all of our measured f and R differences. This possibility is difficult to test by following QCM measurement, since the monomer aggregates fragment even upon gentle handling for SEM preparation. We expect that the polymerized aggregates, which exhibit $\Delta f - \Delta R$ properties of a viscoelastic material, would bring about greater solution viscosity properties, through shear wave energy dissipation, than that produced by the unpolymerized possibly shorter monomer aggregates, accounting for the final response close to that of the pure $(\rho_L \eta)^{1/2}$ line.

Conclusions

We have demonstrated that novel QCM f and R measurements can be made as the pH-dependent binding kinetics and 24 h equilibrium binding levels of DEDT monomer rodlike aggregates are followed at the QCM surface. From these data, a pK_{app} can be estimated for the deprotonation of the α-NH_2 group and subsequent aggregation of DEDT. Upon adding horseradish peroxidase, then H_2O_2, the enzymatic polymerization of the DEDT monomers can be followed through measurement of the f and R shifts. Polymerization results in an increase in viscoelastic behavior in the unpolymerized DEDT monomer aggregates bound to the QCM surface. The final state of the aggregates effects the QCM f and R in a manner closely approaching that of a Newtonian fluid pure viscosity−density effect. These results suggest that the QCM technique has valuable applications to the monitoring and characterization of rodlike, if not all micellar systems. Where polymerization reactions are carried out, significant changes in viscoelastic properties from the initial to the final polymerized state can be easily observed for the surface aggregates. The above results, obtained on a turbid micellar system, represent a significant technical advantage that the inexpensive QCM approach possesses over other characterization techniques.

Acknowledgment

The authors acknowledge support from a Seed Grant from the Research Foundation at the University of Massachusetts Lowell and from NIH Grant R21 GM58583 to K.A.M.

References and Notes

(1) Dunford, B. H. Horseradish Peroxidase: Structure and Kinetic Properties. In *Peroxidases in Chemistry and Biology II*; Everse, J., Everse, K. E., Grisham, M. B., Eds.; CRC Press: Boca Raton, FL, 1990; pp 1−24.

(2) Dordick, J. S.; Marletta, M. A.; Klibanov, A. M. Polymerization of Phenols Catalyzed by Peroxidase in Nonaqueous Media. *Biotechnol. Bioeng.* **1987**, *30*, 31−36.

(3) Ryu, K.; Stafford, D. R.; Dordick, J. S. Peroxidase-Catalyzed Polymerization of Phenols. *ACS Symp. Ser.* **1989**, *389*, 141−152.

(4) Akkara, J. A.; Senecal, K. J.; Kaplan, D. L. Synthesis and Characterization of Polymers Produced by Horseradish Peroxidase in Dioxane. *J. Polym. Sci.* **1991**, *29*, 1561−1574.

(5) Ryu, K.; Dordick, J. S. How do Organic Solvents Affect Peroxidase Structure and Function? *Biochemistry* **1992**, *31*, 2588−2598.

(6) Uyama, H.; Kurioka, H.; Kaneko, I.; Kobayashi, S. Enzymatic Oxidative Polymerization of Alkylphenols. *Macromol. Rapid Commun.* **1994**, *15*, 507−512.

(7) Akkara, J. A.; Ayyagari, M.; Bruno, F. F.; Samuelson, L. A.; John, V. T.; KArayigitoglu, C.; Tripahty, S. K.; Marx, K. A.; Rao, D. V. G. L. N.; Kaplan, D. L. Biomimetic Membrane and Interface Templates for Enzyme-Based Polymerization Reactions. *Biomimetics* **1994**, *4*, 331−339.

(8) Ayyagari, M. S.; Marx, K. A.; Tripathy, S. K.; Akkara, J. A.; Kaplan, D. L. Controlled Free Radical Polymerization of Phenol Derivatives by Enzyme catalyzed Reactions in Organic Solvents. *Macromolecules* **1995**, *28*, 5192−5197.

(9) Bruno, F. F.; Akkara, J. A.; Samuelson, L. A.; Kaplan, D. L.; Mandal, B. K.; Marx, K. A.; Kumar, J.; Tripathy, S. K. Enzynatic Mediated Synthesis of Conjugated Polymers at the Langmuir trough air−water interface. *Langmuir* **1995**, *11*, 889−892.

(10) Sarma, R.; Alva, K. S.; Marx, K. A.; Tripathy, S. K.; Akkara, J. A.; Kaplan, D. L. Enzymatic polymerization of amphiphilic alkyl tyrosine derivatives from emulsions. *Mater. Sci. Eng. C* **1996**, *4*, 189−192.

(11) Alva, K. S.; Sarma, R.; Marx, K. A.; Kumar, J.; Tripathy, S. K. Biochemically Designed Polymers as Self Organized Materials. *SPIE Smart Mater. Technol.* **1997**, *3040*, 200−210.

(12) Marx, K. A.; Sarma, R.; Alva, K. S. Aggregation Properties and SEM Characterization of Decyl esters of Tyrosine. Manuscript in preparation.

(13) Fendler, J. H. In *Membrane-Mimetic Approach to Advanced Materials*; *Advances in Polymer Science 113*; Springer-Verlag: Heidelberg, 1994; pp 62−75.

(14) Sauerbray, G. Verwendung von Schwingquartzen zur Wagung dunner Schichten und zur microwagung (Application of The Quartz Crystal for The Weighing of Thin Films and for Microweighing). *Z. Phys.* **1959**, *155*, 206−222.
(15) Bruckenstein, S.; Shay, M. In situ weighing study of the mechanism for the formation of the adsorbed oxygen monolayer at a gold electrode. *J. Electroanal. Chem.* **1985**, *188*, 131−136.
(16) Bruckenstein, S.; Shay, M. Experimental Aspects of Use of the Quartz Crystal Microbalance in Solution. *Electrochim. Acta* **1985**, *30*, 1295−1300.
(17) Kaufman, J. H.; Kanazawa, K. K.; Street, G. B. Gravimetric Electrochemical Voltage spectroscopy: In situ Mass Measurements during Electrochemical Doping of the Conducting Polymer Polypyrrole. *Phys. Rev. Lett.* **1984**, *53*, 2461−2464.
(18) Nomura, T.; Watanabe, M.; West, T. S. Behavior of Piezoelectric Quartz Crystals in solutions with Application to the Determination of Iodide. *Anal. Chim. Acta* **1985**, *175*, 107−116.
(19) Lu, C.; Czaderna, A. W. *Applications of Piezoelectric Quartz Crystal Microbalances*; Elsevier: New York, 1984.
(20) Buttry, D. A.; Ward, M. D. Measurements of Interfacial Processes at Electrode Surfaces with the Electrochemical Quartz Crystal Microbalance. *Chem. Rev.* **1992**, *92*, 1355−1379.
(21) Ward, M. D. Principles and Applications of the Electrochemical Quartz Crystal Microbalance. In *Physical Electrochemistry, Principles, Methods and Applications*; Marcel Dekker: 1995; pp 293−338.
(22) Kanazawa, K. K.; Gordon, G. The Oscillation Frequency of a Quartz Resonator in contact with a Liquid. *Anal. Chim. Acta* **1985**, *175*, 99−105.
(23) Muramatsu, H.; Kimura, K. Quartz Crystal Detector for Microrheological Study and Its Application to Phase Transition Phenomena of Langmuir−Blodgett Films. *Anal. Chem.* **1992**, *64*, 2502−2507.
(24) Muramatsu, H.; Egawa, A.; Ataka, T. Reliability of correlation between mass change and resonant frequency change for a viscoelastic-film-coated quartz crystal. *J. Electroanal. Chem.* **1995**, *388*, 89−92.
(25) Si, S. H.; Zhou, T.; Liu, D. Z.; Nie, L.; Yao, S. Using Piezoelectric Quartz Crystal to Study Hemorheological Phenomena: Blood Clotting and Urokinase Activated Fibrinolysis. *Anal. Lett.* **1994**, *27*, 2027−2037.
(26) Zhou, T.; Nie, L.; Shouzhou, Y. On equivalent circuits of piezoelectric quartz crystals in a liquid and liquid properties. *J. Electroanal. Chem.* **1990**, *293*, 1−18.
(27) Fawcett, N.; Evans, J. A.; Chien, L.; Flowers, N. Nucleic Acid Hybridization Detected by Piezoelectric Resonance. *Anal. Lett.* **1988**, *21*, 1099−1114.
(28) Su, H.; Yang, M.; Kallury, K. M. R.; Thompson, M. Interfacial Nucleic Acid Hybridization Studied by Random Primer ^{32}P Labelling and Liquid Phase Acoustic Network Analysis. *Anal. Chem.* **1994**, *66*, 769−777.
(29) Su, H.; Williams, P.; Thompson, M. Platinum Anticancer Drug Binding to DNA Detected by Thickness Shear Mode Acoustic Wave Sensor. *Anal. Chem.* **1995**, *67*, 1010−1013.
(30) Ito, K.; Hashimoto, K.; Ishimori, Y. Quantitative analysis for solid-phase hybridization reaction and binding reaction of DNA binder to hybrids using a quartz crystal microbalance. *Anal. Chim. Acta* **1996**, *327*, 29−35.
(31) Muratsugu, M.; Kurosawa, S.; Kamo, N. Detection of Antistreptolysin O Antibody: Application of an Initial Rate Method of Latex Piezoelectric Immunoassay. *Anal. Chem.* **1992**, *64*, 2483−2487.
(32) Ghouechian, H. O.; Kamo, N.; Hosokawa, T.; Akitaya, T. Improvement of Latex Piezoelectric Immunoassay: Detection of Rheumatoid Factor. *Talanta* **1994**, *41*, 401−406.
(33) Thompson, M.; Arthur, G. L.; Dhaliwal, G. K. Liquid Phase Piezoelectric and Acoustic Transmission Studies of Interfacial Immunochemistry. *Anal. Chem.* **1986**, *58*, 1206−1209.
(34) Chang, H. C.; Yang, C. C.; Yeh, T. M. Detection of lipopolysaccharide binding peptides by the use of a lipopolysaccharide coated piezoelectric crystal biosensor. *Anal. Chim. Acta.* **1997**, *340*, 49−54.
(35) Fukuoka, S.; Karube, I. Influence of Cationic Antibiotics on Phase Behavior of Rough Form Lipopolysaccharide. *Appl. Biochem. Biotechnol.* **1994**, *49*, 1−9.
(36) Rickert, J.; Weiss, T.; Kraas, W.; Jung, G.; Gopel, W. A New Affinity Biosensor: Self-Assembled Thiols as Selective Monolayer Coatings of Quartz Crystal Microbalances. *Transducers 95, Eurosensors IX*, **1995**, 528−531.
(37) Imai, S.; Mizuno, H.; Suzuki, M.; Takeuchi, T.; Tamiya, E.; Mashige, F.; Ohkubo, A.; Karube, I. Total urinary protein sensor based on a piezoelectric quartz crystal. *Anal. Chim. Acta.* **1994**, *292*, 65−70.
(38) Matsuda, T.; Kishida, A.; Ebato, H.; Okahata, Y. Novel Instrumentation Monitoring In situ Platelet Adhesivity with a Quartz Crystal Microbalance. *ASAIO J.* **1992**, *38*, 171−173.
(39) Redepenning, J.; Schlesinger, T. K.; Mechalke, E. J.; Puleo, D. A.; Bizios, R. Osteoblast Attachment Monitored with a Quartz Crystal Microbalance. *Anal. Chem.* **1993**, *65*, 3378−3381.
(40) Gryte, D. M.; Ward, M. D.; Hu, W. S. Real Time Measurement of Anchorage Dependent Cell Adhesion Using the Quartz Crystal Microbalance. *Biotechnol. Prog.* **1993**, *9*, 105−108.
(41) Nivens, D. E.; Chambers, J. Q.; Anderson, T. R.; White, D. C. Long-Term On-Line Monitoring of Microbial Biofilms Using a Quartz Crystal Microbalance. *Anal. Chem.* **1993**, *65*, 65−69.
(42) Zhou, T.; Braunhut, S. J.; Medeiros, D.; Marx, K. A., Cellular Adhesion and Spreading of Endothelial Cells Monitored in Real Time Using the Quartz Crystal Microbalance. In *Drug Delivery, Implants and Tissue Engineering*; Materials Research Society Press: Warrendale, PA, 1999; Vol. 50, in press.
(43) Cantor, C. R.; Schimmel, P. R. In *Biophysical Chemistry, I The Conformation of Biological Macromolecules*; W. H. Freeman & Co.: San Francisco, CA, 1980; pp 44−50.
(44) Ebersole, R. C.; Foss, F. P.; Ward, M. D. Piezoelectric Cell Growth Sensor. *Biotechnology* **1991**, *9*, 450−454.
(45) Muramatsu, H.; Tamiya, E.; Karube, I. Computation of equivalent circuit parameters of quartz crystals in contact with liquids and study of liquid properties. *Anal. Chem.* **1988**, *60*, 2142−2150.

Accepted March 11, 1999.

BP990038J